



HAL
open science

Actomyosin contraction induces droplet motility

Thomas Le Goff, Benno Liebchen, Davide Marenduzzo

► **To cite this version:**

Thomas Le Goff, Benno Liebchen, Davide Marenduzzo. Actomyosin contraction induces droplet motility. *Biophysical Journal*, 2020, 119 (5), pp.1025-1032. 10.1016/j.bpj.2020.06.029 . hal-03174993

HAL Id: hal-03174993

<https://amu.hal.science/hal-03174993>

Submitted on 19 Mar 2021

HAL is a multi-disciplinary open access archive for the deposit and dissemination of scientific research documents, whether they are published or not. The documents may come from teaching and research institutions in France or abroad, or from public or private research centers.

L'archive ouverte pluridisciplinaire **HAL**, est destinée au dépôt et à la diffusion de documents scientifiques de niveau recherche, publiés ou non, émanant des établissements d'enseignement et de recherche français ou étrangers, des laboratoires publics ou privés.

Actomyosin contraction induces droplet motility

T. Le Goff,^{1,*} B. Liebchen,^{1,2,†} and D. Marenduzzo^{1,‡}

¹*SUPA, School of Physics and Astronomy, University of Edinburgh,
Peter Guthrie Tait Road, Edinburgh, EH9 3FD, UK*

²*Institute for Theoretical Physics II: Soft Matter, Heinrich-Heine University Düsseldorf,
Universitätsstrasse 1, 40225, Düsseldorf, Germany*

While cell crawling on a solid surface is relatively well understood, and relies on substrate adhesion, some cells can also swim in the bulk, through mechanisms that are still largely unclear. Here, we propose a minimal model for in-bulk self-motility of a droplet containing an isotropic and compressible contractile gel, representing a cell extract containing a disordered actomyosin network. In our model, contraction mediates a feedback loop between myosin-induced flow and advection-induced myosin accumulation, which leads to clustering and a locally enhanced flow. Interactions of the emerging clusters with the droplet membrane break flow symmetry and set the whole droplet into motion. Depending mainly on the balance between contraction and diffusion, this motion can be either straight or circular. Our simulations and analytical results provide a framework allowing to study in-bulk myosin-driven cell motility in living cells and to design synthetic motile active matter droplets.

PACS numbers:

Introduction – Understanding the rules governing cell motion is a fascinating problem in biophysics, because the engine governing motility is purely self-organised [1, 2]. The mechanism of cell motility is also of major biomedical relevance, as this process is central to the self-assembly of tissues in a growing embryo, is required for wound healing, and is important to understand the pathway through which cancer cells metastasise.

Crawling on a solid substrate [1–6] is the motility mode currently best characterised, both experimentally and theoretically. It requires polymerisation of the actin cytoskeletal network, which pushes the cell forward by ratcheting the motion of its plasma membrane [7]. For this mechanism to work, the actin cytoskeleton needs to be anchored to the substrate at least transiently, to avoid back-slip of the whole network following polymerisation. Indeed, anchoring points are well documented for crawling cells: these are “focal adhesions”, formed by clusters of transmembrane proteins binding to the substrate [2, 5]. This mechanistic understanding of cell crawling has been described in various successful models, quantitatively explaining, in particular, the locomotion of keratocyte cells on a substrate [8, 9].

Crucially, however, some cells can even move through tissue or the extracellular matrix [10], where we have no underlying substrate. Cancer cells invading a 3D matrix have a spherical morphology, possess no lamellipodium, and show an accumulation of actin at their back [11, 12] rather than the front, making it unlikely that actin polymerisation is directly responsible for cell locomotion. This example suggests that the mechanism for in-bulk cell motion, which is not understood in detail [10], must be fundamentally different from that of crawling in 2D. The challenge of moving in absence of a substrate can be appreciated by comparing the mechanism allowing birds to fly through 3D space, with that

exploited by animals to walk on the ground.

Our goal in this work is to provide a model and mechanism for cell motility in bulk, which is both minimal and generic. Since myosin is currently the best candidate to provide the engine for 3D cell motility, through some form of ATP-dependent contractility [13, 14], we model *isotropic* contraction of an actomyosin gel confined in a droplet, mimicking a cell or a cell extract (i.e., a bag of actomyosin enclosed by a membrane, without regulatory proteins). Previous work proposed related models of contractility-induced motility [13–18]: these studies, however, either invoked the rectification of splay fluctuations in droplets of *anisotropic* active nematic gels [13, 15, 16], or considered additional ingredients besides an actomyosin droplet, such as a thin cortex to which motors can bind dynamically [16], or a frictional substrate [14, 17]. In our minimal model, the mechanism for in-bulk motility is provided by contractility, favouring myosin clustering, and steric interaction with the enclosing membrane, breaking the symmetry of the density field spatially. We find two modes of in-bulk motility, associated with either linear, or circular motion.

Model – To model in-bulk cell motility we describe a subcellular actomyosin gel as an isotropic active gel with a stress tensor,

$$\bar{\sigma} = \mu [\nabla \mathbf{v} + (\nabla \mathbf{v})^T] + [\lambda (\nabla \cdot \mathbf{v}) + \mathcal{X} f(m)] \mathbb{I}, \quad (1)$$

where \mathbf{v} is the velocity field of the active gel, μ is its dynamic viscosity, λ the bulk viscosity and \mathcal{X} measures myosin-induced contraction. The strength of contractility depends on the concentration of myosin motors, m , as $f(m) = \frac{m}{1+m}$, ensuring saturation at large m [20]. As actomyosin is contractile, $\mathcal{X} > 0$. [Note Eq. 1 disregards passive contributions, which we assume negligible with respect to active ones as in [14].]

To model myosin transport, we use an advection-diffusion equation. Here, the local advection velocity of myosin may be different from that of the active gel, since motors can dynamically attach and detach from actin filaments with rate depending on the environment [21]. We therefore introduce the dimensionless parameter $\alpha_m \in [0, 1]$ to quantify the affinity of myosin with actin, where $\alpha_m = 1$ means all motors are permanently attached to the actomyosin gel. Additionally, force balance (where inertial terms can be neglected at cellular scales) yields the following equations of motion for the myosin density field $m(\mathbf{x}, t)$ and the actomyosin velocity field $\mathbf{v}(\mathbf{x}, t)$:

$$\begin{cases} \partial_t m = -\alpha_m \nabla \cdot (m \mathbf{v}) + D_m \nabla^2 m, \\ \gamma v_x = (2\mu + \lambda) \partial_x^2 v_x + \mu \partial_y^2 v_x + (\mu + \lambda) \partial_x \partial_y v_y \\ \quad + \mathcal{X} \partial_x f(m), \\ \gamma v_y = (2\mu + \lambda) \partial_y^2 v_y + \mu \partial_x^2 v_y + (\mu + \lambda) \partial_x \partial_y v_x \\ \quad + \mathcal{X} \partial_y f(m), \end{cases} \quad (2)$$

where D_m is the myosin diffusion coefficient and γ the friction coefficient which is $\neq 0$ only with an underlying substrate. We formulated our model in 2D to allow for systematic parameter sweeps – extension to 3D is straightforward and should lead to analogous results.

To reduce the parameter space to its essential dimensions, we now use $t_u = \mu/\mathcal{X}_0$ and $x_u = \sqrt{D_m \mu/\mathcal{X}_0}$ as time and space units where \mathcal{X}_0 is a reference value for contractility. We also introduce dimensionless parameters $\eta \equiv \lambda/\mu$ (ratio of bulk and dynamic viscosity), $\chi \equiv \mathcal{X}/\mathcal{X}_0$ (contraction strength), $\Gamma \equiv D_m \gamma/\mathcal{X}_0$ (reduced substrate friction, which vanishes without a substrate), and use the dimensionless fields $\tilde{m} = m/m_0$ (where m_0 is the average actomyosin density which is conserved under the dynamics) and $\tilde{\mathbf{v}} = \sqrt{\frac{\mu}{D_m \mathcal{X}_0}} \mathbf{v}$.

Inspired by previous works [22, 23], we use a phase-field approach to model enclosure of actomyosin within a membrane, to mimic a cell or cell extract. Thus, we define a phase field $\phi(\mathbf{x}, t)$ and a corresponding equation of motion featuring two fixed points representing locally uniform phases: $\phi \approx 1$, representing the interior of the cell, and $\phi \approx 0$, representing the space outside it.

In dimensionless units and in presence of the phase field, our minimal model reads (omitting tildes):

$$\begin{cases} \partial_t m = -\alpha_m \nabla \cdot (m \mathbf{v}) + \nabla^2 m + \epsilon_m \nabla^2 \left(\frac{\delta \mathcal{E}}{\delta m} \right), \\ \Gamma v_x = (2 + \eta) \partial_x^2 v_x + \partial_y^2 v_x + (1 + \eta) \partial_x \partial_y v_y \\ \quad + \chi \partial_x f(m), \\ \Gamma v_y = (2 + \eta) \partial_y^2 v_y + \partial_x^2 v_y + (1 + \eta) \partial_x \partial_y v_x \\ \quad + \chi \partial_y f(m), \\ \partial_t \phi = D_\phi \nabla^2 \phi - \Gamma_\phi U'(\phi) - \mathbf{v} \cdot \nabla \phi, \end{cases} \quad (3)$$

Here, we have introduced $\mathcal{E}(m, \phi) = \iint d\mathbf{r} \{ (m^2 + \alpha) [(1 - \phi)^2 + \alpha] \}^{1/2}$ as an effective energy to constrain myosin within the cell boundaries. The diffusivity D_ϕ quantifies the ability of the cell to oppose deformation, hence we call it deformation resistance. Its effect is similar to surface tension, which would, however, enter the equations

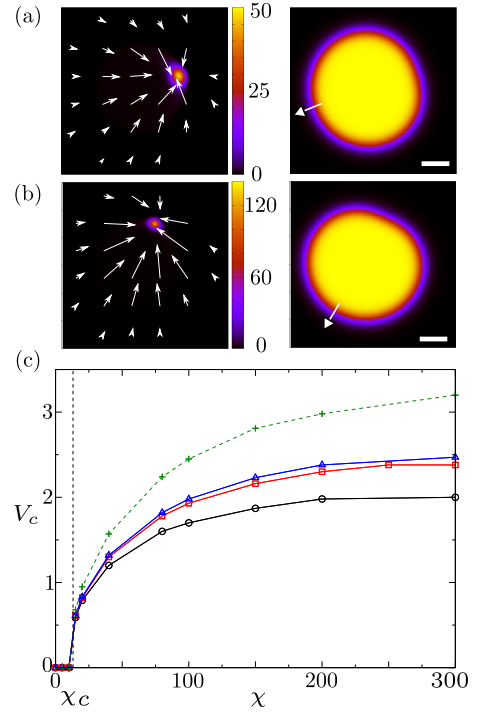


FIG. 1: (a,b) Left: concentration of myosin and \mathbf{v} -field for $V_{tar} = 12.5$, $D_\phi = 20$, $\alpha_m = 1$ and $\gamma = 0$. Right: corresponding phase field. The white arrow gives the direction of cell motion and the scale bar is 1. The contractility is $\chi = 80$ in (a) and $\chi = 200$ in (b). (c) Overall cell velocity as a function of χ . The solid lines corresponds to simulations without solid friction and the dashed-line corresponds to simulations with $\gamma = 0.2$. Black line and circles: $D_\phi = 10$; red line and squares: $D_\phi = 20$; blue line triangles: $D_\phi = 25$; green dashed line and crosses: $D_\phi = 25$.

of motion in a formally different way [32, 33]. The term $U'(\phi) = \phi(\phi - 1)[\phi - \frac{1}{2} - \alpha_0(\frac{V}{V_{tar}} - 1)]$, is the derivative of the double-well potential U whose fixed points $\phi = 0$ and $\phi = 1$ describe the outside and inside of the cell extract. The droplet interface (cell boundary) has a characteristic width of $(8D_\phi/\Gamma_\phi)^{1/2}$. The term $\alpha_0(\frac{V}{V_{tar}} - 1)$ restores the instantaneous cell volume $V = \iint d\mathbf{r} \phi^2(3 - 2\phi)$ towards a characteristic target volume V_{tar} . Finally, $-\mathbf{v} \cdot \nabla \phi$ represents the advection of the actomyosin network.

To get an intuition for the order of magnitude of our model parameters, we set experimentally relevant length, time and viscosity scales for cell extracts and actomyosin droplets as $x_u \sim 1 \mu\text{m}$, $t_u \sim 1 \text{s}$, and $\mu \sim 10 \text{ Pa}\cdot\text{s}$ [25, 29]. These give $D_m \sim 1 \mu\text{m}^2 \text{s}^{-1}$, and $\mathcal{X}_0 \sim 10 \text{ Pa}$ – the former value is close to the *in vivo* myosin diffusion coefficient, to gauge the latter we note a myosin concentration of $m_0 \sim 1 - 10 \mu\text{M}$ [24, 25] and a force per motor of 10 pN [25–27] creates a contractility of $\mathcal{X} \sim 3 - 30 \mathcal{X}_0 \text{ Pa}$ (calculated assuming a myosin size $\sim 50 \text{ nm}$ [1]).

Contractility induced cell-motility – To explore the dynamics of actomyosin droplets, we simulate Eqs. (3). As parameters, we use $\eta = -2/3$ [31], $\epsilon_m = 20$, $\alpha = 10^{-4}$

and $\alpha_0 = 50$. We choose $D_\phi/\Gamma_\phi = 160$, to fix the shape and width of the cell boundary throughout our simulations. We also set $\Gamma = 0$ to study in-bulk motility, $m_0 = 1$, and choose initial conditions as $m = m_0 + \delta m$ and $\mathbf{v} = \delta \mathbf{v}$ where δm and $\delta \mathbf{v}$ represent small fluctuations.

We first consider the limit where myosin has a strong affinity with actin ($\alpha_m = 1$). For small contractility χ , the myosin remains uniform within the cell, which is stationary. However, when the contractility surpasses a threshold, a myosin spot forms at one edge of the cell (Figs. 1a,b and Suppl. Movie 1 [34]). While this spot grows, the cell deforms. Strikingly, it then starts to move away from the myosin spot, which now sits at its rear. Soon, the cell reaches a constant velocity and moves along a straight line (Suppl. Movie 1 [34]).

Although we do not directly model the underlying solvent flow, a viable pattern is one in which it opposes actomyosin flow, to ensure that the whole system (actomyosin plus solvent) is incompressible. This is a realistic flow pattern as, at the timescales we consider, membranes can be regarded as permeable, hence solvent can move in and out of a cell extract freely [35–37].

To better understand the parameter dependence of the droplet velocity, we now perform a systematic parameter scan: as a result, we find that the droplet speed not only increases with contractility but also with the deformation resistance D_ϕ (Fig. 1(c)), so that stiff circular cells move faster than easily deformable ones. Intriguingly, we also find a moderate friction with a substrate, $\Gamma > 0$, increases the droplet speed whereas strong friction ($\Gamma \gg 1$) entirely suppresses motion as we shall see below.

To understand the instability mechanism leading to contractility-induced motility, as well as the threshold value for χ , we now perform a linear stability analysis. Considering an infinite system first, i.e. $\phi \equiv 1$, we find the following dispersion relation (Fig. 2a,b), describing the growth rate of small fluctuations around the uniform phase as a function of the wavenumber q [34]:

$$\lambda(\mathbf{q}) = \mathbf{q}^2 \left(\frac{\alpha_m \chi m_0}{(1 + m_0)^2 [\Gamma + (2 + \eta) \mathbf{q}^2]} - 1 \right). \quad (4)$$

Linear instability of the uniform phase occurs when (the real part of) $\lambda(\mathbf{q})$ is positive for some wavevector \mathbf{q} (in Fig. 2A, this corresponds to the red and the dark yellow curves), which leads to the instability criterion

$$\frac{\alpha_m \chi m_0}{\Gamma(1 + m_0)^2} > 1. \quad (5)$$

This result shows that the uniform phase is unstable to patterning if χ is strong enough (or simply if it is > 0 in absence of friction, Fig. 2B). Increasing m_0 initially promotes the instability, but too large a value restores the uniform phase.

Extending our stability analysis to the case where a nonuniform phase field is present, we find that the above

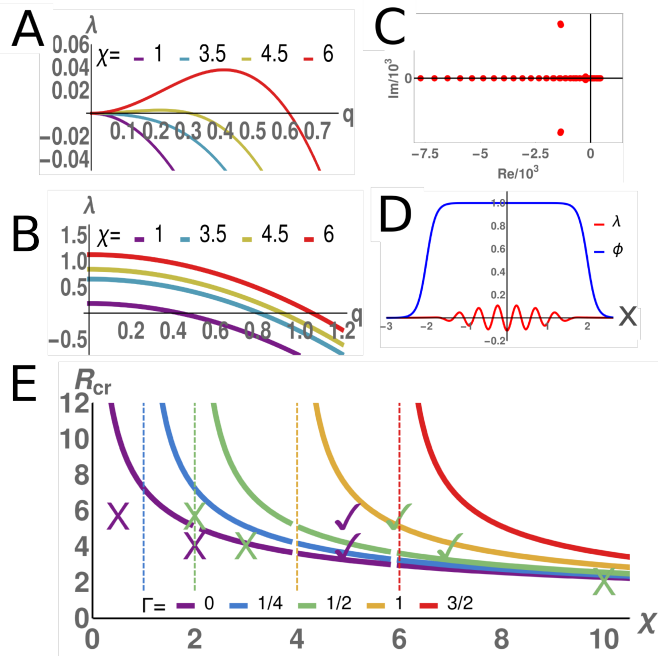


FIG. 2: Linear stability analysis: (A,B): $\phi = 1$ (no droplet confinement); growth rate $\lambda(q)$ of small fluctuations around the uniform phase with friction [$\Gamma = 1$, (A)] and without [$\Gamma = 0$, (B)]. (C,D): $\phi \neq 1$: Red dots show eigenvalues $\lambda_1 \dots \lambda_N$ whose real parts determine the growth rate of actomyosin-fluctuations within a droplet. Dots right of the $\text{Re} = 0$ -line represent unstable modes; the fastest growing one is shown in panel (D) and represents instability within the droplet and its suppression at the droplet boundaries, meaning that contractility-induced cell-motility can only occur in large enough cells (see SM [34] for details). Parameters: $\chi = 4.5$; $R = \sqrt{V/\pi} = 2$ and $L = 3$; $dx = 0.01$; $N = 601$ (for discretization); others as in simulations. Panel (E) shows the corresponding (phase) χ -dependent critical cell radii for different friction values. Symbols \checkmark (cell motion) and \times (no motion) show agreement with numerical simulations and dashed lines show critical χ values, below which contractility-induced motility is impossible, even for very large cells.

criterion still holds, but only if the cell is sufficiently large (see [34] for details). In fact, as visualized in Fig. 2(D), the fastest growing mode (panel C), is localised in the center of the cell and gets suppressed at the boundaries. If the droplet is too small, the boundary suppression destroys myosin patterns, and the droplet is stationary. We quantify this argument by requiring that the shortest possible unstable wavelength (e.g. for the red line in panel A this is about $l \approx 2\pi/0.62$) is smaller than the diameter of the cell ($2R$) to allow for myosin accumulation within the droplet (and hence droplet motion). Through Eq. (4), this leads to the critical contractility

$$\chi_c = \frac{(1 + m_0)^2}{\alpha_m m_0} \left[\Gamma + (2 + \eta) \left(\frac{\pi}{R} \right)^2 \right]. \quad (6)$$

For the parameters used in simulations presented in Fig. 1 ($V_{tar} = 12.5$ and $\alpha_m = 1$), the critical contractility is

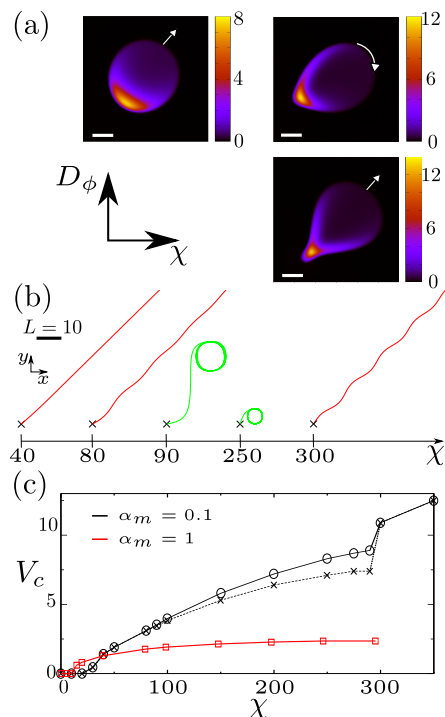


FIG. 3: Simulation results for $V_{tar} = 12.5$, $\Gamma = 0$ and $\alpha_m = 0.1$. (a) Left top panel: myosin profile for $\chi = 80$ and $D_\phi = 20$. Right top panel: myosin profile for $\chi = 200$ and $D_\phi = 20$. Right bottom panel: myosin profile for $\chi = 200$ and $D_\phi = 5$. Scale bar is 1. (b) Different trajectories of the droplet center depending on χ for $D_\phi = 20$. (c) Velocity of the droplet as a function of contraction χ for $D_\phi = 20$. The black solid line with circles corresponds to the droplet center of mass, the black dashed line with crosses to the myosin center of mass. The red curves with squares corresponds to $\alpha_m = 1$.

$\chi_c \leq 13.2$ with $\Gamma = 0$ and $\chi_c \leq 14$ with $\Gamma = 0.2$, in good agreement with our numerics. We show predictions from Eq. (6) in panel E and compare it with simulations. Eq. 6 – in dimensional units – suggests that key control parameters are $\frac{\chi}{\gamma D_m}$, for $\gamma \neq 0$, and $\frac{\chi R^2}{\mu D_m}$, for $\gamma = 0$: when these are large enough, the contractile isotropic droplet moves.

Circular droplet motion – We now explore the case of low affinity between myosin and actin, $\alpha_m < 1$, again for $\Gamma = 0$. In this case, our droplets do not always swim straight, but may follow oscillatory trajectories or lock into a regular circular motion, depending on the value of χ and D_ϕ (see Fig. 3a).

What is the mechanism underlying deviations from a linear droplet motility? For $\alpha_m < 1$ myosin is advected slower than the actin network, whose speed is approximately equal to the overall cell velocity. As a consequence of its slower speed, the myosin spot, which is elliptical for large α_m (Fig. 1a,b), reshapes into a crescent-like form (see Fig. 3a), which is a consequence of myosin accumulation at the lateral cell boundaries. As we increase χ , the crescent becomes longer and thinner. Crucially, for our noisy initial conditions the crescent ‘grows’ asym-

metrically at both sides of the cell. This asymmetric growth results in a torque, since contraction takes place along the myosin concentration gradient, which pulls the cell perpendicular to its direction of motion, leading to curved motion. Remarkably, as the cell moves faster than myosin the curved motion further enhances the asymmetry of the crescent: thus, a sufficiently strong initial asymmetry of the crescent triggers a positive feedback loop between crescent asymmetry and cell-turning rate ultimately yielding circular motion. This mechanism is only valid for a relatively undeformed cell. If D_ϕ is small, the cell can respond to the emerging torque simply by deforming, disrupting the feedback loop described above. This picture is in line with our simulations showing that for $\alpha_m < 1$ and small D_ϕ the droplet forms a tail at the rear confining the myosin spot and hampering the formation of a large and asymmetric crescent (Fig. 3a).

It is instructive to explore the droplet velocity V_c as a function of χ for $\alpha_m < 1$ (Fig. 3(c)). For $\alpha_m = 0.1$ the contractility threshold before cell motion sets in is much larger than for $\alpha_m = 1$, as predicted by ((6)). Interestingly, beyond this threshold, the reduced actin-myosin affinity leads to faster droplet motion. Finally, for strong contraction, when we reach the regime of circular motion, the velocity of the center of mass of the myosin cluster is smaller than V_c . This means that the myosin center of mass is closer to the middle of the trajectory than the cell center, consistent with our physical argument for circular motion.

To get a more comprehensive overview of the parameter regimes leading to straight, oscillatory or circular cell motion, we systematically performed a large number of simulations for different parameter regimes, and summarize our results in two phase diagrams, depending on χ, D_ϕ for in-bulk motility, $\Gamma = 0$ (Fig. 4(a)), and on χ, Γ for motion with friction ($\Gamma \neq 0$, Fig. 4(b)). These diagrams show three different phases: (i) quiescent, (ii) rectilinear motion and (iii) circular motion. We find that friction favours rectilinear motion over circular one in a similar way as large deformation resistance does.

Conclusions – In conclusion, we have proposed a generic mechanism exploiting motor-induced contractility to yield in-bulk motility of an isotropic actomyosin droplet. In-bulk motility arises when contractile stresses exceed a threshold scaling inversely with the cell size – hence, even a very weak contractility may be enough to propel large droplets. While our mechanism is independent of the presence of a substrate, we have shown that wall-contact may both enhance the droplet speed or entirely suppress motion, subtly depending on parameters.

Our in-bulk cell motility mechanism may apply to the motion of cells through 3D tissues *in vivo*, or through matrigel *in vitro*. It may also serve as a framework to design contractility-powered self-motile synthetic actomyosin droplets in the lab such as in [38]. Directly testable predictions of our work include the speed-up of

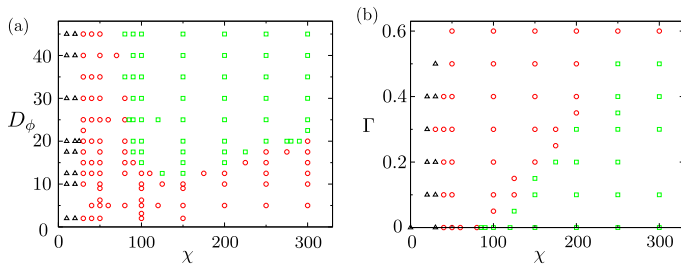


FIG. 4: (a) $\chi - D_\phi$ phase diagram for $\alpha_m = 0.1$ and $\Gamma = 0$. Black triangles, red circles and green squares respectively denote stationary cells, straight and curved motion. (b) $\chi - \Gamma$ phase diagram for $\alpha_m = 0.1$ and $D_\phi = 25$.

motion with increasing contractility and stiffness, and the stabilization of oscillatory (circular) motion for large enough isotropic contractile stresses.

We thank EPSRC (grant EP/J007404/1) for support. BL gratefully acknowledges received funding by a Marie Skłodowska Curie Intra European Fellowship (G.A. no 654908) within Horizon 2020.

* Electronic address: thomas.le-goff@ed.ac.uk

† Electronic address: liebchen@hhu.de

‡ Electronic address: dmarendu@ph.ed.ac.uk

- [1] D. Bray, *Cell Movements*, 2nd ed., Garland Publishing, New York (2001).
- [2] R. Phillips, J. Kondev and J. A. Theriot, *Physical biology of the cells*, Garland Science, New York (2008).
- [3] S. Schaub, S. Bohnet, V.M. Laurent, J.-J. Meister, and A.B. Verkhovsky, *Mol. Biol. Cell.* **18**, 3723 (2007).
- [4] J. Stricker, T. Falzone, and M.L. Gardel, *J. Biomech.* **43**, 9 (2010).
- [5] E. L. Barnhart, K. C. Lee, K. Keren, A. Mogilner and J. A. Theriot, *PLoS Biol.* **9**, e1001059 (2011).
- [6] T.L. Goff, B. Liebchen, D. Marenduzzo, *Phys. Rev. Lett.* **117**, 238002 (2016).
- [7] C. S. Peskin, G. M. Odell and G. F. Oster, *Biophys. J.* **65**, 316 (1993).
- [8] K. Kruse, J.-F. Joanny, F. Jülicher, and J. Prost, *Phys. Biol.* **3**, 130 (2006).
- [9] C. W. Wolgemuth, J. Stajic and A. Mogilner, *Biophys. J.* **101**, 545 (2011).
- [10] S. Evan-Ram and K. M. Yamada, *Curr. Opin. Cell. Biol.* **17m** 524 (2005).
- [11] H. Keller, A.D. Zadeh, and P. Eggli, *Cell Motil. Cytoskeleton* **53**, 189 (2002).
- [12] R. Poincloux, O. Collin, F. Lizarraga, M. Romao, M. Debray, M. Piel and P. Chavrier, *Proc. Natl. Acad. Sci. USA* **108**, 1943 (2011).
- [13] E. Tjhung, D. Marenduzzo and M. E. Cates, *Proc. Natl. Acad. Sci. USA* **109**, 12381 (2012).
- [14] P. Recho, T. Putelat, and L. Truskinovsky, *Phys. Rev. Lett.* **111**, 108102 (2013).
- [15] C. A. Whitfield, D. Marenduzzo, R. Voituriez and R. J. Hawkins, *Eur. Phys. J. E* **37**, 8 (2014).
- [16] C. A. Whitfield, and R. J. Hawkins, *New J. Phys.* **18**, 123016 (2016).
- [17] M. Nickaen, I.L. Novak, S. Pulford, A. Rumack, J. Brandon, B.M. Slepchenko, and A. Mogilner, *PLOS Comput. Biol.* **13**, e1005862 (2017).
- [18] Just before finishing this manuscript, [17] has been published which is technically similar to the present manuscript, but focuses on the biology of cell-motility close to frictional substrates, whereas we focus on novel physical mechanisms allowing for in-bulk cell motility.
- [19] J.S. Bois, F. Jülicher, and S.W. Grill, *Phys. Rev. Lett.* **106**, 028103 (2011).
- [20] T. Moore, S.K. Wu, M. Michael, A.S. Yap, G.A. Gomez, and Z. Neufeld, *Biophys. J.* **107**, 2652 (2014).
- [21] R.S. Adelstein, and E. Eisenberg, *Ann. Rev. Biomech.* **49**, 921 (1980).
- [22] D. Shao, H. Levine, and W.-J. Rappel, *Proc. Natl. Acad. Sci. USA* **109**, 6851 (2011).
- [23] A. Dreher, I.S. Aranson, and K. Kruse, *New J. Phys.* **16**, 055007 (2014).
- [24] L.W. Janson, J. Kolega, and D.L. Taylor, *J. Cell Biol.* **114**, 1005 (1991).
- [25] M. Norstrom, and M.L. Gardel, *Soft Matter* **7**, 3228 (2011).
- [26] J. T. Finer, R.M. Simmons, and J.A. Spudich, *Nature* **368**, 113 (1994).
- [27] P.M. Bendix, G.H. Koenderink, D. Cuvelier, Z. Dogic, B.N. Koeleman, W.M. Brieher, C.M. Field, L. Mahadevan, and D.A. Weitz, *Biophys. J.* **98**, 3126 (2008).
- [28] D.H. Wachsstock, W.H. Schwarz, and T.D. Pollard, *Biophys. J.* **66**, 801 (1994).
- [29] F. Wottawah, S. Schinkinger, B. Lincoln, R. Ananthkrishnan, M. Romeyke, J. Guck, and J. Käs, *Phys. Rev. Lett* **94**, 098103 (2005).
- [30] S.M. Volkmer Ward, A. Weins, M.R. Pollak, and D.A. Weitz, *Biophys. J.* **95**, 4915 (2008).
- [31] G.K. Batchelor, *An Introduction to Fluid Dynamics* (Cambridge Univ. Press, Cambridge, 2000), p.144.
- [32] R. Folch, J. Casademunt, and A. Hernández-Machado, and L. Ramírez-Piscina, *Phys. Rev. E* **60**, 1724 (1999).
- [33] T. Biben, and C. Misbah, *Phys. Rev. E* **67**, 031908 (2003).
- [34] See online Supplementary Material at XXX for Supplementary Movies, and some linear stability analyses of our equations of motion.
- [35] R. Fettiplace, and D.A. Haydon, *Physiol. Rev.* **60**, 510 (1980).
- [36] J.C. Mathai, S. Tristram-Nagle, J.F. Nagle, and M.L. Zeidel, *J. Gen. Physiol.* **131**, 69 (2008).
- [37] W. Shinoda, *Biochim. Biophys. Acta Biomembr.* **1858**, 2254 (2016).
- [38] Y. Nishigami, H. Ito, S. Sonobe and M. Ichikawa, *Scientific Reports* **6**, 18964 (2015).